

| | |
|-----------------------------|---|
| Title | Structural analysis of a roof extracted from a wind turbine blade |
| Authors | Gentry, T. Russell;Al-Haddad, Tristan;Bank, Lawrence C.;Arias, Franco R.;Nagle, Angela;Leahy, Paul G. |
| Publication date | 2020-12 |
| Original Citation | Gentry, T. R., Al-Haddad, T., Bank, L. C., Arias, F. R., Nagle, A. and Leahy, P. (2020) 'Structural Analysis of a Roof Extracted from a Wind Turbine Blade', Journal of Architectural Engineering, 26(4), 04020040. doi: 10.1061/(ASCE)AE.1943-5568.0000440 |
| Type of publication | Article (peer-reviewed) |
| Link to publisher's version | https://ascelibrary.org/doi/pdf/10.1061/%28ASCE%29AE.1943-5568.0000440 - 10.1061/(ASCE)AE.1943-5568.0000440 |
| Rights | © 2020, American Society of Civil Engineers. This material may be downloaded for personal use only. Any other use requires prior permission of the American Society of Civil Engineers. The published article may be found at https://ascelibrary.org/doi/pdf/10.1061/%28ASCE%29AE.1943-5568.0000440 |
| Download date | 2024-04-25 07:42:49 |
| Item downloaded from | https://hdl.handle.net/10468/11171 |



UCC

University College Cork, Ireland
 Coláiste na hOllscoile Corcaigh

STRUCTURAL ANALYSIS OF A ROOF EXTRACTED FROM A WIND TURBINE BLADE

T. Russell Gentry¹, Tristan Al-Haddad², Lawrence C. Bank³, DistM. ASCE,
Franco R. Arias⁴, Angela Nagle⁵, Paul Leahy⁶

Abstract

The objective of this research is to demonstrate that parts of decommissioned wind turbine blades can be repurposed for infrastructure applications for a sustainable future of the wind power industry. The purpose of this paper was to develop a methodology to conduct detailed structural engineering design of composite material parts extracted from wind turbine blades. A large section extracted from a 100 meter long blade was repurposed as a roof for a small (approximately 40 m²) single-story masonry house. Geometric and material properties were taken from the blade design documents. A 3-D graphical model was created from the exterior surface and material layups. The roof was designed using the Load and Resistance Factor

¹ Associate Professor, School of Architecture, Georgia Institute of Technology, 245 4th St NW, Atlanta, GA 30332, USA russell.gentry@design.gatech.edu

² Lecturer, School of Architecture, Georgia Institute of Technology, Atlanta, 245 4th St NW, GA 30332, USA tristan.al-haddad@formations-studio.com

³ Research Faculty, School of Architecture, Georgia Institute of Technology, 245 4th St NW, Atlanta, GA 30332, USA larry.bank@design.gatech.edu (corresponding author)

⁴ Former Graduate Student, Civil Engineering Department, City College of New York, 160 Convent Av, New York, NY 10031, USA farias.civeng@gmail.com

⁵ Graduate Student, Civil, Department of Civil, Structural and Environmental Engineering, University College Cork, College Road, Cork, Republic of Ireland
AngelaJaneNagle@umail.ucc.ie

⁶ Lecturer, Energy Engineering, University College Cork, College Road, Cork, Republic of Ireland paul.leahy@ucc.ie

(LRFD) method familiar to civil engineers. Analysis of stresses and deflections was conducted using hand calculations and the finite element method (FEM). The results of the analyses show that the roof is within code mandated stress and deflection limits. The methodology developed can be applied to other wind blade repurposing concepts.

Keywords: Recycling, Repurposing, Design, Finite element analysis, Wind turbine blades,

Introduction

Fiber Reinforced Polymer (FRP) composite materials are not biodegradable and present unique problems for waste management and their End-of-Life (EOL). The impact of polymers on the environment and society has become a major concern in many countries. In response to the European Waste Directive (DIRECTIVE 2008/98/EC, 2008), the option of disposing of end-of-life FRP blades in landfills is now restricted by landfill taxes and reuse, recycling and recovery targets. Since the 1990s, there has been a developing body of research that has studied the issues of recycling and EOL of FRP composites, in general, and composite wind blades, in particular. Recent analyses of the key issues related to the EOL of wind turbine blades can be found in Liu and Barlow (2017), Jensen and Skelton (2018) and Bank et al. (2018). For example, a typical 2.0 MW turbine with three 50 m blades has approximately 20 tonnes of FRP material and an 8 MW turbine has approximately 80 tonnes of FRP material (based on a conservative 1 MW \approx 10 tonnes of FRP conversion). Based on a predicted “moderate growth scenario” from the Global Wind Energy Council (GWEC), waste blades from future wind power installations will total of 16.8 million tonnes by 2030 and 39.8 million tonnes by 2050 if no action is taken in the interim

(GWEC, 2016). At the present time numerous large (40 to 60 meter) composite material wind turbine blades are coming out of service due to their original 20-year design life or due to replacement by more efficient turbines and/or blades (referred to as repowering).

Managing Composite Material “Waste”

There are various methods to manage waste composites (either production waste or EOL waste products) at the present time (Oliveux et al., 2015, Job et al, 2016) – some of which are referred to as “recycling”. Unfortunately, the term “recycling” has many different meanings in this field and the term “second-life” is preferred so there is a clear understanding of their position in a waste processing hierarchy. Following Skelton (2017) and Jensen and Skelton (2018) we propose the following categorization of second-life options for FRP wind blades;

1. **Reuse:** In this scenario the entire blade is reused. The blade is used as a turbine blade in its second life but has its lifetime extended by refurbishment or remanufacturing or is sold on the second-hand market.
2. **Repurpose:** In this scenario the structural properties and the material properties of the composite are repurposed. The blade is used whole or sectioned into parts and repurposed for other products such as parts of temporary or inexpensive housing, office and home furniture, benches and playgrounds, pedestrian bridges and powerline structures (Bank et al., 2018; Adamcio, 2019; Bladesign, 2019; SuperuseStudios, 2012; Speksnijder, 2018; Suhail et al., 2019; Anmet, 2019; Bank et al, 2019; Alshannaq et al, 2019).
3. **Recycle**

a. **Fully-Recycle:** In this scenario the material properties of the composite are recycled.

The blade is cut, shred or ground into small pieces or granular material as filler for use in concrete or other composites (Beauson et al, 2016; Mamanpush et al, 2018; Yazdanbakhsh et al, 2018; Rodin et al., 2018).

b. **Partially-Recycle:** In this scenario the glass fiber constituent of the composite is used. This includes thermo–chemical methods such as pyrolysis, solvolysis, thermolysis (fluidized bed) (Oliveux et al 2015) that are used to reclaim the glass fiber. Or the glass fiber is used as a feedstock for cement clinker by co-processing the shredded composite material in a cement kiln (Ramesh et al 2018).

Waste disposal methods such as landfilling or incineration, with or without energy recovery, or syngas production are not considered to be second-life methods since no material is reused in a new product. Clearly, all the second-life methods listed above will need “third-life” or other disposal methods in the future. In most of the world landfilling is the predominant method of disposing of FRP scrap and EOL waste costing in the range of \$45 to \$200 per ton. With the increased awareness of the environmental impacts of climate change, decreased and more expensive natural resources, and greater global concerns for health, the barriers to FRP production and waste disposal are likely to increase.

In what follows the repurposing of a part extracted from a 100 m long FRP blade as a roof structure is discussed. Fig. 1 shows conceptual designs for platform foundations, doors and window shutters, roof panels and roof for small (approx. 40 m²) masonry block houses (Bank et al, 2018.) Such buildings are ubiquitous in the developing world. Of the different possible uses

of the blade parts shown in Fig. 1, the roof was chosen for further detailed structural analysis because of its large size and complex geometry and materials. The study follows and expands a prior conceptual study of a similar roof structure with different geometry and calculations (Bank et al, 2019.)

Wind Blade Geometry

The wind blade selected for the current work was a 100 m long prototype wind blade designed by Sandia National Laboratories (SNL) identified as SNL-100-01 (Griffith, 2013). This blade is similar in size to a 107-meter turbine blades currently being manufactured for a 12 MW turbine (General Electric, 2019). The geometry is defined by 25 different airfoils at specific stations along the blade length from the root end, where the blade is connected to the turbine hub, to the tip. The materials are defined by 393 different solid and sandwich composite material lay-ups. The SNL-100-01 model of the blade is a two-dimensional wire frame (surface) model built using the Numerical Manufacturing and Design Tool (NuMAD) (Berg and Resor, 2012, Arias, 2016). A three-dimensional architectural model of the blade including thickness and material types at all locations is required for architectural and structural calculations and detailing. Fig. 2. shows the three-dimensional model of the 100-meter blade which was built from the stack layups and material types provided in Griffith (2013) using Rhino 3D (Rhino, 2017, Arias, 2017)

The blade has a maximum chord (i.e., the distance between the leading edge and trailing edge) of 7.628 m at a distance of 19.5 m from the root end. The blade has a foam core shell, three internal foam core webs (identified as SW1, SW2 and SW3 from left to right in Fig. 2(b)) and a carbon

fiber spar cap (shown in black above and below the webs SW1 and SW2). The part of the 100 meter blade that was extracted from the three-dimensional blade model to create the roof region was extracted from Station 19 to Station 20 (27.6 m to 35.8 m) and is shown schematically in Fig. 3.

A schematic rendering of the part used for the roof is shown on the masonry block walls of the approximately 40 m² house in Fig. 4. Fig. 4 also shows schematics of the connection details using Simpson Strong-Tie[®] straps between the blade roof and the masonry walls. Fig. 4 also shows schematics of louvre type window shades to enclose the open ends of the blade roof. Louvre type windows and shades are commonly used in informal housing in developing countries where high humidity and temperatures are common (Bank et al 2018)

Structural Analysis of the Roof

Dimensions

The center-line dimensions of the roof used in the calculations that follow are shown in Fig. 5.

Materials

The mechanical and physical properties of the materials as well as their layups in different locations around the cross-section and along the length of the SNL-100-01 blade are given in Griffith (2013). These are based on the MSU material test database (Mandell et al 1997, SNL

2019). In cases where properties were not provided in Griffith (2013) they were obtained from the literature as noted in Table 1.

The geometric and material properties of the roof were determined for the laminates and sandwich panels for the region from Station 19 to Station 20 (27.6 m to 35.8 m). These were used in both hand calculations and in the LS-DYNA finite element method (FEM) analysis in what follows. The as-reported properties given in Griffith were used in the analysis. Any changes in material properties or dimensions due to the expected 20-year in-service operation of the blade were not considered at this time. The estimation of residual properties in wind blades after 20 years of service (known as remaining-life) is an active research field (Post et al 2008).

Design Philosophy

For civil engineering structural analysis of composite material structures the Load and Resistance Factor Design (LRFD) (or its equivalent called Limit States Design (LSD) in the EU) methods or Allowable Stress Design (ASD) methods are used (Bank, 2006). The two primary limit states analyzed are the Ultimate Limit State (ULS) and the Serviceability Limit State (SLS). In the ultimate limit state (strength, stability) analysis, nominal service loads are typically increased using prescribed load factors and the structural or material capacities are typically reduced using prescribed resistance or materials safety factors. In the serviceability limit state (deflections, vibrations etc.), neither the nominal service loads nor the material properties are typically factored. The loads for the ULS and SLS are referred to as the factored loads or the service loads, respectively.

154

155 Nominal service live loads and load combinations (load cases) are used for a civil engineering
156 structural design and are stipulated in ASCE 7-16 (2016) or Eurocode EN 1991: Actions on
157 structures (1991). Load combinations are factored amounts of nominal dead load, live load, roof
158 live load, wind load, snow load, and others (ASCE 7-16).

159

160 The resistance or material factors depend on the type of materials used and are given in separate
161 material specific design codes (e.g., for concrete, the ACI 318-19 or EN 1992: Design of
162 concrete structures; CEN 1992) At the time of writing (2019) an approved design code does not
163 exist for composite materials for civil engineering structures. An ASCE Standard and a Eurocode
164 are currently under development. In the absence of a code the material factors for the FRP
165 materials used in this analysis are taken from EUR (2016), the precursor document to the
166 Eurocode. The Material Partial Factor, γ_M , for ultimate strength was calculated to be $\gamma_M = (1.15$
167 $\times 1.35 \times 1.2) = 1.86$, assuming (1) the material properties were obtained by test ($\gamma_{M1} = 1.15$), (2)
168 the production processes and properties of the materials have a standard deviation ≤ 0.10 ($\gamma_{M2} =$
169 1.35), and, (3) be the material was not post-cured ($\gamma_{M3} = 1.2$).

170

171 For the serviceability analysis the nominal service loads are used and the Material Partial Factor,
172 $\gamma_M = 1.0$. For most structures the serviceability requirements are set by building codes (e.g.,
173 International Building Code (IBC 2018)). For roof structures the requirement is typically that the
174 deflection, δ , (displacement downwards due to gravity) be $\delta < L/240$ (i.e., the member span
175 divided by 240)

176

It is also of interest to note that design codes for composite wind blades themselves are not yet available. Technical Committee TC 88, working group PT 61400-5 of the International Electrotechnical Commission (IEC) is currently working on IEC 61400 - Part 5: Rotor blades. However, even when these codes are published, they will not be suitable for structural design for civil structures since local authorities provide construction permits for projects based on building codes such as the International Building Code (ICC, 2018) which incorporate the model material design codes (e.g., ACI-318).

Loads for roof design

For the purposes of the proof-of-principle analysis presented in this paper only one load combination was considered: Dead Load + Roof Live Load ($D + L_r$). Only a uniform dead load was considered. Concentrated live load, wind, snow or ice load on the roof load were not considered at this time. This was done to demonstrate the methodology needed for such calculations. It is important to note that other load cases especially those related to wind loads also need to be analyzed. Wind load can create uplift on a roof system which could affect not only the design of the roof itself but, perhaps more significantly, the design of the connection details and louvres shown in Fig. 4.

The dead load was determined by uniformly distributing the entire 24.32 kN weight of the roof (determined from the material densities and volumes) over the entire projected roof area of 42.9 m². This gave a uniformly distributed dead load, $D = 0.566 \text{ kN/m}^2$. The code stipulated roof live

load, $L_r = 0.96 \text{ kN/m}^2$ was used. This gives an unfactored service load of 1.52 kN/m^2 and a factored load of $1.2(0.566) + 1.6(0.96) = 2.212 \text{ kN/m}^2$ (ASCE 7-16 LRFD load combination 3).

Preliminary Analysis - Hand calculations

Hand calculations using one-dimensional mechanics of materials models were used to determine stresses in individual elements of the roof – Case (1) the shell panel between the 2nd shear web and the trailing edge, and Case (2) the third shear web of the roof section. These two cases were chosen for the hand calculations since they were found to be those that gave the largest local deflections and stresses in the roof structure based on a prior approximate analysis conducted (Bank et al 2019). Simplifying assumptions were made relative to the boundary conditions of the shell and web sandwich panels in order to obtain a rough order of magnitude (ROM) estimate of the stresses prior to conducting the detailed FEM analysis described in the following section. Such analyses are routinely made in the early conceptual design stages by structural engineers and architects.

(1) Out-of-Plane Bending of the Shell Panel

The sandwich panel at the chosen location in the blade consists of a 60 mm thick thermoplastic foam core and two 5 mm composite material face skins of SNLTriax (see Table 1). Since this shell panel is in the transverse (contour) orientation relative to the blade (and roof) longitudinal axis the transverse stiffness and strength properties of the materials are used: $E_{22(\text{Triax})} = 13.65$

GPa, $E_{\text{foam}} = 0.256$ GPa, $\sigma_{22(\text{Triax})} = +144$ MPa, $\sigma_{22(\text{Triax})} = -213$ MPa, $\sigma_{\text{tens}(\text{foam})} = +3.1$ MPa,
 $\sigma_{\text{comp}(\text{foam})} = -3.8$ MPa, and $\tau_{\text{ult}(\text{foam})} = 2.0$ MPa (see Table 1).

The shear web sandwich panels consist of a 60 mm thick thermoplastic foam core and two 3 mm composite material face skins of SNLBiax (see Table 1). Since the shear web sandwich panels are parallel to the blade (and roof) longitudinal axis the longitudinal stiffness and strength properties of the materials are used: $E_{11(\text{biax})} = 13.60$ GPa, $E_{\text{foam}} = 0.256$ GPa, $\sigma_{11(\text{Biax})} = +144$ MPa and $\sigma_{11(\text{Biax})} = -213$ MPa.

The critical shell panel for analysis was assumed to span between the second web and the trailing edge over the third web as shown in Fig 6. It was analyzed as a flat continuous beam of unit width (1 m) over three supports: S1 second web (0.9 m); S2 third web (0.6m); and S3 the trailing edge. The end supports at the trailing edge and the second web (0.90 m deep) were assumed to be pinned while the middle support (0.60 m web) was assumed to be an elastic spring support with a stiffness equal to the in-plane stiffness of the web. The spans were 1.81 m and 1.94 m respectively.

Using the transformed section method the SNLtriax skins were transformed into the properties of the core ($n_1 = 13.65/0.256 = 53.3$) to give a transformed second moment of the 70 mm thick shell panel of $I_{t(\text{shell})} = 5.82 \times 10^8 \text{ mm}^4$. For the 600 mm deep shear web 3 the SNLBiax skins were transformed to the properties of the core ($n_2 = 13.60/0.256 = 53.1$) to give a transformed second moment of the 600 mm deep web of $I_{t(\text{web})} = 6.84 \times 10^9 \text{ mm}^4$. The flexural stiffness of the shell is calculated as, $E_c I_{t(\text{shell})} = 1.49 \times 10^{11} \text{ N.mm}^2$ and that of the web $E_c I_{t(\text{web})} = 1.75 \times 10^{12} \text{ N.mm}^2$.

Solving the indeterminate structure in Fig. 6 for the contact force, R_2 , between the shell and the web gives the support reactions due to factored loads, $R_1 = R_3 = 2694$ N, $R_2 = 2876$ N. The maximum moment occurs at $x = 1223$ mm from S1 and is equal to $M_{\max} = 1.64 \times 10^8$ N-mm. The maximum shear force is $V_{\max} = 2694$ N. The maximum tensile and compressive stresses in the top shell skin is $\sigma_{\text{Triax_skin}} = \pm 5.26$ MPa and the core of $\sigma_{\text{foam}} = \pm 0.085$ MPa. The shear stress in the core is $\tau_{\text{foam}} = 2694/(60)(1000) = 0.045$ MPa. The downward deflection of shell due to service loads at R_2 was $\delta = 12.08$ mm.

(2) In-plane Bending of the Shear Web

The 600 mm deep by 8000 mm long web is loaded by a tributary area of half the distance (1.81 m) to SW2 on the left side and half the distance (1.94 m) to the trailing edge on the right side as shown in Fig. 7. The web is assumed to be simply-supported at its two ends (spanning between the short-end walls of the house) and connected to the shell at its top edge. It is analyzed as a T-beam. The effective width of the T-beam flange is taken as $b_{\text{eff}} = b_{\text{web}} + 16(t_{\text{shell}}) = 66 + 16(70) = 1186$ mm which is less than $L/4 = 2000$ mm or the web spacing, $S = 1810$ mm (ACI 318-19).

For this configuration the SNLTriax skin is in its longitudinal direction and the longitudinal stiffnesses and strength properties are used: $E_{11(\text{Triax})} = 27.7$ GPa, $\sigma_{11\text{tens}(\text{Triax})} = +972$ MPa, $\sigma_{11\text{comp}(\text{Triax})} = -702$ MPa. Properties of the shear web and the foam are as in Case (1) above.

Using the transformed section method the SNLTriax and SNLTriax skins were transformed into the properties of the core ($n_1 = 27.7/0.256 = 108.2$, $n_2 = 13.60/0.256 = 53.1$) above giving $\bar{Y} = 589$ mm from the bottom of the web and $I_t = 2.90 \times 10^{10}$ mm⁴. The uniform line load (factored)

on the top of the web was calculated to be 4.16 N/mm. The maximum bending moment at midspan assuming simple supports at the 8-m ends was $M_{\max} = 3.31 \times 10^7$ N-mm and the maximum shear force at the supports was $V_{\max} = 16,640$ N. The maximum positive and negative flexural stresses at midspan were $\sigma_{\text{Triax_top}} = -10.06$ MPa, $\sigma_{\text{Biax_bot}} = +36.06$ MPa, $\sigma_{\text{foam_shell}} = -0.087$ MPa, $\sigma_{\text{foam_web}} = -0.680$ MPa, $\tau_{\text{foam_web}} = 0.462$ MPa (assuming the web foam core carries all the shear force). The maximum displacement (deflection) under service loads at midspan was 29.9 mm. (span/268).

If the T-beam web is assumed to be fixed-fixed at its ends the maximum deflection is 5.98 mm (span/1338) and the maximum stresses at midspan (positive moment) are: In the panel Triax skin $\sigma_{\text{Triax_top}} = -3.35$ MPa and in the web Biax skin $\sigma_{\text{Biax_bot}} = +12.01$ MPa, and the maximum stresses at the fixed support (negative moment) in the panel Triax skin $\sigma_{\text{Triax_top}} = +6.71$ MPa and in the web Biax skins $\sigma_{\text{Biax_bot}} = -24.02$ MPa (all four stresses need to be determined since the section is unsymmetric and both positive and negative moment regions exist.)

Overdesign Factor – Hand Calculations

Comparing the calculated stresses and displacements to the material strengths and the code specified deflection limits ($L/240$ in this case) indicates the amount of overdesign. It is important to note that this not the safety factor which is accounted for in the load and material factors used. Ideally the structural designer attempts to get the overdesign factor (ODF) as close as possible to 1.0. In the current repurposing design the structure and its properties are predetermined by the original design (as a wind blade) and the stresses and deflections are checked with allowable

values. The properties of the section cannot be changed as in a typical design iteration (although they can be modified with local stiffeners and strengtheners). The architectural design is performed at the conceptual stage where the repurposing concept is developed for different sizes of blades. Hence the structural analysis is done to verify the acceptability of stresses, deflections and overdesign factors as opposed to the safety factors that need to be reported. The level of overdesign for the two cases considered above is presented separately for purposes of discussion but, in reality, the lowest number obtained is the actual overdesign factor for the entire structure.

The calculated stresses and displacements and their relevant allowable values and overdesign factors for Case 1 are shown in Table 2. The critical stress for the shell panel is the tensile stress in the transverse direction SNLTriax material in the top layer; but the ODF = 14.7 is high which indicates low utilization of the material capacity. However, the deflection is closer to the code requirement with an ODF = 1.29. Since all overdesign factors are > 1.0 the shell panel has sufficient strength and stiffness under this loading condition. For large glass fiber composite material structures, it is common that serviceability conditions control the design (Bank, 2006).

The calculated stresses and displacements and their relevant allowable values and overdesign factors for Case 2 are shown in Table 3. The critical stress for the shell panel is the tensile stress in the longitudinal direction of the SNLBiax material in the web skins, with an ODF = 2.1. The foam core critical shear stress in the web has an ODF = 2.4. Again, the serviceability condition controls the design with an ODF = 1.1. Nevertheless, all ODFs are > 1.0 for these hand-calculations and the structure is safe and serviceable. Note that the results shown in Table 3 for the shear web are for the less conservative analysis that assumes that the shear web is pin-roller

supported (as opposed to fixed-fixed) at its ends. ODFs will be higher if the fixed-fixed conditions are used.

Detailed analysis – finite element method

The finite element modeling of the roof was conducted using the implicit version of the LS-DYNA software code (LS-DYNA, 2018). LS-DYNA implicit was chosen because the authors have detailed knowledge and many years of experience working with this code (both the implicit and explicit forms (e.g., Bank and Gentry (2001)). Unfortunately, finite-element codes of this type are not ideally suited to structural engineering analysis since they do not allow “automatic” evaluations of standard ASCE 7 load cases. This means that the load cases must be input manually which is not trivial. Equally unfortunate is that standard structural engineering design codes (e.g., ETABS, STAAD, ROBOT) do not permit arbitrary laminated composite plate and shell elements.

The FEM mesh, global (X, Y, Z) and local (x, y, z) coordinate systems for the shell and the webs, and the boundary conditions are shown in Fig. 8. In Fig. 8 triangles represent pinned supports and circles roller supports and grey circles indicate support hidden from view in this orientation. The colors in the model represent different layups in segments of the blade that were used in the roof. The foreshortened perspective shown in Fig. 8 is drawn looking from the 35.8 m station towards the 27.6 m station (i.e., tip to root of the blade).

The yellow region is the Carbon Fiber Reinforced Polymer (CFRP) / Glass Fiber Reinforced Polymer (GFRP) spar cap between webs 1 and 2 (5 mm SNLTriax/80 mm SNLCarbon/5 mm SNLTriax), the green regions are the GFRP/foam shell sandwich panel (5 mm SNLTriax/60 mm foam/5 mm SNLTriax), the brown region is the trailing edge panel (TE) (5 mm SNLTriax/15 mm Glass UD/40 mm Foam/5 mm SNLTriax), and the blue regions are the SNLBiax/foam web panels (3 mm SNLBiax/50 mm foam/3 mm SNLBiax) (Griffith, 2013). A fully-integrated laminated shell element (LSDYNA ELFORM=16) was used. The total model consisted of 3115 nodes and 1813 elements. The major 11-axis of the materials (see Table 1) is aligned with the global Y-direction and the local x -direction for the shell and web segments (see Fig. 8).

Results of Finite Element Analysis

Selected results from the finite element analyses are presented to illustrate the stress distributions and displacements in key locations. As in the hand calculations the factored load in the global Z-direction was 2.212 kN/m^2 . This was uniformly distributed over the 3115 nodes in the model. Fig. 9 shows the vertical displacement (deflection) of the roof in the negative Z-direction. The maximum displacement of 7.1 mm (downwards) occurs over the 3rd shear web near the center of the large panel between the trailing edge support and the 2nd shear web.

The stress at the midplane of the top surface in the SNLTriax layer in the skin of the shell sandwich panel in the local y -direction is shown in Fig. 10. To help with visualization the shear webs are only shown in outline in these contour plots. The maximum compressive stress in the transverse direction of -5.0 MPa occurs in the two panels on either side of the 3rd shear web. It

be can be seen that the 3rd shear web provides a flexible intermediate support and the compressive stress decreases along this line giving the butterfly shaped stress contours. The light blue shading over the 2nd shear web indicates a tensile stress and a negative curvature (and moment) over the support. Regions of high tensile stress in the shell top skin are also seen at the upper ends of the 3rd shear web indicating negative curvature at the end of the flexible intermediate support and some fixity at the ends provided by shell action.

The stress at the midplane of the top surface in the SNLTriax layer in the skin of the shell sandwich panel in the local x -direction is shown in Fig. 11. (In this figure the stress along the blade axis is shown, σ_x , while in Fig. 10 the stress transverse to the blade axis is shown, σ_y . Due to two-way bending of the panel these stresses are different.) As with the y -direction the central portion is in compression (green) with a maximum longitudinal compressive stress in this region of -5.0 MPa. Similar to the y -direction tensile stresses are seen in the x -direction at the ends of the 3rd shear web indicating a negative curvature in this direction as well. However, this is not as significant as in the x -direction due to the higher stiffness of the shell skin laminate in the x -direction.

The displacements and stress in the shear webs are shown next. To help with visualization the shell panels are only shown in outline in these contour plots. Downwards displacement of the shear webs is shown in Fig. 12. The maximum deflection in the Z -direction is 7.1 mm (downwards) and occurs under the 3rd shear web which is equal to the deflection of the top shell at this location shown in Fig. 9. This to be expected as the in-plane deformation of the shear

webs in the Z-direction is negligible. The maximum displacement under the 2nd shear web is significantly less and is 2.4 mm at its center. This explains the restraint provided by the 2nd shear web and the negative curvature over the webs seen in Fig. 10. The 1st shear web which is fully supported at its bottom along the wall shows no downward displacement, as expected.

The stresses in the x-direction in the shear webs are shown in Fig.13. The maximum tensile stress occurs in the SNLBiax skin in the 3rd shear web at the bottom of the web and is equal to 10.9 MPa. Tensile stresses at the bottom of the 2nd shear web are less, with a maximum at the center of 5.7 MPa. It is interesting to note the relatively large compressive stresses of -25.0 MPa at the pinned supports of the shear webs. This implies a localized outward thrust due to a global restraint provided by the shell. It is important to note the shear webs are supported by roller supports (no restraint in the longitudinal X-direction) at their far ends (see Fig. 8) so ideally there should be no thrust at the pinned supports at the near ends. However, the shear webs do not behave as simple beams and are restrained at their ends by the global two-way action of the shell.

The stresses in the local y-direction of the shear webs are shown in Fig. 14. Compressive stresses are noted at the supports which are larger at the near ends due to the pinned support as noted previously.

Finally, elastic buckling analysis was conducted to check for overall instability of the roof structure. The buckling occurs at a load magnification factor of 31 (i.e., 31 times the factored load of 2.212 kN/m².) Buckling occurs in the 3rd shear web as is shown in Fig. 15. This is logical given the large compressive stresses seen in this location in both the local x and y directions.

However, the buckling load is much larger than would be required to cause material failure in these locations and elastic instability will be precluded. Nevertheless, local stiffening will be needed at the supports of the 2nd and 3rd webs to prevent both local bearing failure and local buckling at these locations (Borowicz and Bank 2013).

Overdesign Factor – 3-D FEM Calculations

The finite element analysis gives results for the entire structure unlike the hand-calculations where the shell and web were analyzed separately. The results for the 3-D FEM calculations are given in Table 4.

The critical stress for the roof as a whole is the compressive stress in the longitudinal direction in the SNLBiax layer in the shear web with an ODF = 4.6. All ODFs are all greater than 1.0 for this FEM analysis and the structure is safe. The critical displacement is in the shell panel with an ODF of 2.2 which satisfies serviceability requirements.

Discussion

The results obtained from the one-dimensional mechanics-of-materials hand calculations and the full three-dimensional finite element method analyses are in reasonably good agreement. Generally, the stresses and deflections obtained from the FEM analysis are less than those obtained in the hand-calculations. This is to be expected as the roof shell has a two-way action that distributes loads in both the transverse and longitudinal directions. It is encouraging to know

that provided good modeling assumptions are made for hand-calculations, these calculations can be used in preliminary design stages to assess the feasibility of repurposing designs. In addition, the FEM analysis uncovers local multi-directional stresses, especially at the supports, which provides important input for structural detailing such as local stiffening and strengthening.

Conclusions

A methodology for structural analysis of EOL wind turbine blade sections has been developed and demonstrated. This is essential for repurposing wind turbine blades. The methodology can be applied to other structural applications for decommissioned wind turbine blades. This will contribute to improved sustainability of the wind energy sector. As indicated in the paper both hand-calculations and finite element methods can be used for analysis. Nevertheless, this is not trivial as a wind blade tapers and twists and its material properties change along its length. In either case the analysis results will only be as good as the assumptions made in building the analytical models. Over-simplification of hand-calculation models is not advised. When FEM analysis is used laminated shell elements must be used and care must be taken to correctly orient the orthotropic materials in the laminate with respect to the global coordinate system.

For structural analysis and architectural detailing a full 3-D model showing the individual material layers of the blade is needed. However, most blade models used for aerodynamic and structural analysis are wire frame surface models. In addition, for infrastructure applications governing building codes will need to be used since local jurisdictions permit construction based on these codes. These codes are not typically familiar to composite material designers. At the

current time a code does not exist to obtain probabilistically based material partial factors or element resistance factors for design of FRP structures. But, code like documents can be and are used in lieu of these codes.

Acknowledgement

Support for this research was provided by the U.S. National Science Foundation (NSF) under grants 1701413, and 1701694; by InvestNI/Department for the Economy (DfE) under grant 16/US/3334 and by Science Foundation Ireland (SFI) under grant USI-116 (US-Ireland Tripartite program).

Data Availability Statement

Some or all data, models, or code that support the findings of this study are available from the corresponding author upon reasonable request.

References

ACI (American Concrete Institute). 2019. *2019 Building Code Requirements for Structural Concrete*, ACI 318-19. Farmington Hills, MI: ACI

Adamcio, A. 2019. "Usable elements from wind turbine wings." Accessed November 21, 2019.

<https://www.anmet.com.pl/>

472

473 Agarwal, B.H., Broutman, L.J., and Chandrashekhara, K. 2006. *Analysis and Performance of*
474 *Fiber Composites*, 3rd Edition, Pg. 549. Hoboken, NJ: John Wiley & Sons.

475

476 3A Core Materials. 2018. "AIREX[®] T92.200." Accessed November 21, 2019.

477 <https://www.3accorematerials.com/en/products/airex-foam/airex-t92-pet-foam>

478

479 Alshannaq, A., D. Scott, L. Bank, M. Bermek, and R. Gentry. 2019. "Structural re-use of de-
480 commissioned wind turbine blades in civil engineering applications." In Proceedings of the
481 American Society for Composites—Thirty-Fourth Technical Conference on Composite Material,
482 DEStech Publications, Inc. 439 North Duke Street, Lancaster, Pennsylvania 17602-4967 USA,
483 ISBN: 978-1-60595-602-2, USB flash drive or CD-ROM. <https://www.destechpub.com/>

484

485 Arias, F.R. 2016. "NuMAD Modeling and Finite Element Analysis of SNL-100-01 Wind
486 Turbine Blade Shells." Independent Study Report, Department of Civil Engineering, City
487 College of New York, NY. DOI: 10.13140/RG.2.2.18870.04161.

488

489 Arias, F.R. 2017. "Reusing composite materials from decommissioned wind turbine blades." MS
490 Report, Department of Civil Engineering, City College of New York, NY. DOI:
491 10.13140/RG.2.2.30509.23527

492

493 ASCE (American Society of Civil Engineers). 2016. *Minimum Design Loads and Associated*
494 *Criteria for Buildings and Other Structures*. ASCE 7-16. Reston, VA, USA: ASCE

495

496 Bank, L.C. 2006. *Composites for Construction: Structural Design with FRP Materials*,
497 Hoboken, NJ: Wiley

498

499 Bank, L.C. and Gentry, T.R. 2001. "Development of a Pultruded Composite Material Highway
500 Guardrail," *Composites Part A: Applied Science and Manufacturing*, 32(9):1329-1338.

501 [https://doi.org/10.1016/S1359-835X\(01\)00086-0](https://doi.org/10.1016/S1359-835X(01)00086-0)

502

503 Bank, L.C., Arias, F.R., Yazdanbakhsh, A., Gentry, T.R., Al-Haddad, T., Chen, J.F. and
504 Morrow, R. 2018. "Concepts for Reusing Composite Materials from Decommissioned Wind
505 Turbine Blades in Affordable Housing." *Recycling*, 3(1), 3.

506 <https://doi.org/10.3390/recycling3010003>

507

508 Bank, L.C., Arias, F.R., Gentry, T.R., Al-Haddad, T., Tasistro-Hart, B. and Chen, J.F. 2019.
509 "Structural analysis of FRP parts from waste wind turbine blades for building reuse
510 applications," in *Advances in Engineering Materials, Structures and Systems: Innovations,*
511 *Mechanics and Applications*. Edited by A. Zingoni, 1520-1524. Boca Raton, FL: CRC Press.
512 ISBN 9781138386969.

513

514 Beauson, J., Madsen, B., Toncelli, C., Brøndsted, P., Ilsted Bech, J., 2016. "Recycling of
515 shredded composites from wind turbine blades in new thermoset polymer composites." *Compos.*
516 *Part A Appl. Sci. Manuf.* 90, 390–399. <https://doi.org/10.1016/j.compositesa.2016.07.009>

517

Berg, J.C. and Resor, B.R. 2012. *Numerical Manufacturing and Design Tool (NuMAD v2.0) for Wind Turbine Blades: User's Guide*. SAND2012-7028, Sandia National Laboratories, Albuquerque, NM.

Bladesign. 2019. "Products." Accessed November 21, 2019. <https://www.bladesign.de/products>

Borowicz, D.T. and Bank, L.C. 2013. "Effect of web reinforcement on the behavior of pultruded fiber-reinforced polymer beams subjected to concentrated loads." *Const and Bldg Mats*, 14, 347-357. <https://doi.org/10.1016/j.conbuildmat.2013.05.081>

CEN (European Committee for Standardization). 1991. *Actions on structures. Eurocode 1*. Brussels, Belgium: CEN.

CEN (European Committee for Standardization). 1992. *Design of concrete structures. Eurocode 2*. Brussels, Belgium: CEN.

DIRECTIVE 2008/98/EC. 2008. *DIRECTIVE 2008/98/EC OF THE EUROPEAN PARLIAMENT AND OF THE COUNCIL of 19 November 2008 on waste and repealing certain Directives*. 22.11.2008 EN Official Journal of the European Union L 312/3.

EUR (Publications Office of the European Union). 2016. *Prospect for new guidance in the design of FRP*. EUR 27666 EN. Accessed November 21, 2019. <http://publications.jrc.ec.europa.eu/repository/handle/JRC99714>

General Electric. 2019. “[Haliade-x offshore wind turbine platform](https://www.ge.com/renewableenergy/wind-energy/offshore-wind/haliade-x-offshore-turbine).” Accessed November 21, 2019. <https://www.ge.com/renewableenergy/wind-energy/offshore-wind/haliade-x-offshore-turbine>

Griffith, T. 2013. *The SNL100-01 Blade: Carbon Design Studies for the Sandia 100-meter Blade*. SAND2013-1178. Sandia National Laboratories, Albuquerque, NM, USA.

GWEC (Global Wind Energy Council). 2016. *Global Wind Energy Outlook – 2016*. Accessed November 21, 2019. <http://gwec.net/publications/global-wind-energy-outlook/global-wind-energy-outlook-2016/>

ICC (International Code Council) 2018. *International Building Code*. Washington, DC: ICC.

Jensen, J.P. and Skelton, K. 2018. “Wind turbine blade recycling: experiences, challenges and possibilities in a circular economy.” *Ren. & Sust. Energy Reviews*. 97: 165-176.

<https://doi.org/10.1016/j.rser.2018.08.041>

Job, S., Leeke, G., Mativenga, P.T., Oliveux, G., Pickering, S. and Shuaib, N.A. 2016.

[Composites Recycling: Where are we now?](https://compositesuk.co.uk/system/files/documents/Recycling%20Report%202016.pdf) Accessed November 21. 2019.

<https://compositesuk.co.uk/system/files/documents/Recycling%20Report%202016.pdf>

Liu, P. and Barlow, C.Y. 2017. "Wind turbine blade waste in 2050." *Waste Management*, 62: 229-240. <https://doi.org/10.1016/j.wasman.2017.02.007>

LS-DYNA. 2018. Version 4.5.21 May 2018. Livermore Software Technology Corporation, Livermore, CA. www.lstc.com

Mamanpush, S. H., Li, H., Englund, K., and Tabatabaei, A. T. (2018). Recycled wind turbine blades as a feedstock for second generation composites. *Waste Management*, 76, 708-714. doi:10.1016/j.wasman.2018.02.050.

Mandell, J.F., D.D. Samborsky, D.D., 1997. *DOE / MSU Composite material fatigue database. Version 19.0*. Sandia Technical Report, SAND97-3002. Sandia National Laboratories, Albuquerque, NM, USA

Oliveux, G., Dandy, L., and Leeke, G. 2015. "Current status of recycling of fibre reinforced polymers: Review of technologies, reuse and resulting properties." *Prog. in Mat. Sci.* 72: 61-99. <https://doi.org/10.1016/j.pmatsci.2015.01.004>

Post, N.L., Lesko, J.J., and Case, S.W., (2010), "Fatigue Life Prediction of Composites and Composite Structures", in *Fatigue Life Prediction of Composites and Composite Structures*, Woodhead, pp. 79-101. <https://doi.org/10.1533/9781845699796.1.79>

Ramesh, N. Tasneem Abbasi, S. M. Tauseef and S.M., Abbasi, S.A. 2018. "Utilization of fiber-reinforced plastic (FRP) waste generated by a wind-turbine manufacturing company."

International Journal of Engineering & Scientific Research, 6 (2) 103 – 129. Jagadhri, India

Rhino3D. (2018). Rhinoceros V5.0 Educational. Robert McNeel & Associates, Seattle, USA.

www.rhino3d.com

Rodin, H., Somayeh Nassiri, R., Englund, K., Fakron, O., and Li, H., 2018. "Recycled glass fiber reinforced polymer composites incorporated in mortar for improved mechanical performance."

Const. and Build. Mats. 187, 738-751. <https://doi.org/10.1016/j.conbuildmat.2018.07.169>

Skelton, K. 2017. "Discussion paper on managing composite blade waste." WindEurope Technical Report. DOI: 10.13140/RG.2.2.22748.90248.

Speksnijder, S., 2018. "Reuse of wind turbine blades in a slow traffic bridge." Accessed November 21, 2019. <http://www.stijnspeksnijder.com/gallery/bridge-of-blades/>

SNL. 2019. *SNL/MSU/DOE 2019 Composite Material Database, Version 29*. Accessed November 21, 2019. <https://energy.sandia.gov/programs/renewable-energy/wind-power/blade-reliability/mhk-materials-database/>

Suhail, R., Chen, J.-F., Gentry, R., Taristro-Hart, B., Xue, Y., Bank, L., 2019. "Analysis and Design of a Pedestrian Bridge with Decommissioned FRP Windblades and Concrete." In Proc.,

609 *14th Int. Symp. On Fiber-Reinforced Polymer Reinforcement of Concrete Structures*
610 (FRPRCS14), Belfast, UK, Belfast, UK, June 4-7, 2019, paper no. 176. International Institute
611 for FRP in Construction (IIFC), [https://www.iifc.org/publications/proceedings-iifc-official-](https://www.iifc.org/publications/proceedings-iifc-official-conferences/)
612 [conferences/](https://www.iifc.org/publications/proceedings-iifc-official-conferences/)
613
614 SuperuseStudios, 2012. "REwind Willemsplein - Superuse Studios." Accessed November 21,
615 2019. <https://www.superuse-studios.com/projects/rewind-willemsplein/>
616
617 Yazdanbakhsh, A., Bank, L.C., Rieder, K.A., Tian, Y., Chen, C., 2018. "Concrete with discrete
618 slender elements from mechanically recycled wind turbine blades." *Resour. Conserv. Recycl.*
619 128,11-21. <https://doi.org/10.1016/j.resconrec.2017.08.005>
620

List of Figures

- Fig. 1 Repurposing concepts for housing from 100 m long blade parts
- Figure 2. a.) Entire 100-m long blade, b.) Cross-sectional view at Station 19 (27.6-m from the root end)
- Fig. 3 Location of roof section extracted from blade (along the length)
- Fig. 4 Schematic of roof
- Fig. 5 Dimensions of the roof (perspective drawing)
- Fig. 6 Analytical model of the shell panel and supports
- Fig. 7 Analytical model of the shear web and supports
- Fig. 8. FEM mesh and boundary conditions
- Fig. 9. Z-displacement of the roof
- Fig. 10. Stresses in top skin layer in y -direction (blade transverse or contour direction)
- Fig. 11. Stresses in top skin layer in x -direction (blade longitudinal direction)
- Fig. 12 Displacement of the shear webs in the Z -direction
- Fig 13 Stresses in the shear webs in the x -direction (longitudinal direction of the web)
- Fig 14 Stresses in the shear webs in the y -direction (vertical direction in the web)
- Fig. 15 Buckled shape of the 3rd shear web

List of Tables

| |
|---|
| Table 1. Material properties of laminates in the SNL-100-01 |
| Table 2. Hand-Calculation Overdesign Factors (ODFs) for Case 1 – Shell Panel |
| Table 3. Hand Calculation Overdesign Factors (ODFs) for Case 2 – Shear Web (T-Beam) |
| Table 4. 3-D FEM Calculation Overdesign Factors (ODFs) for entire roof |

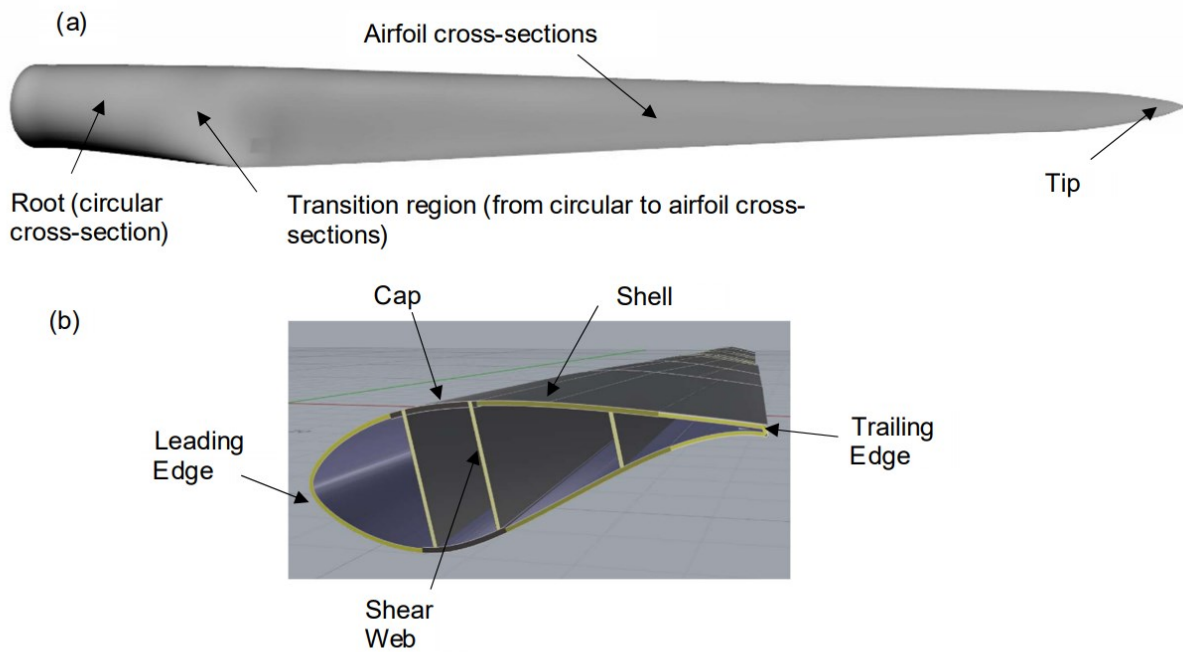
665 Figure 1.



666

667

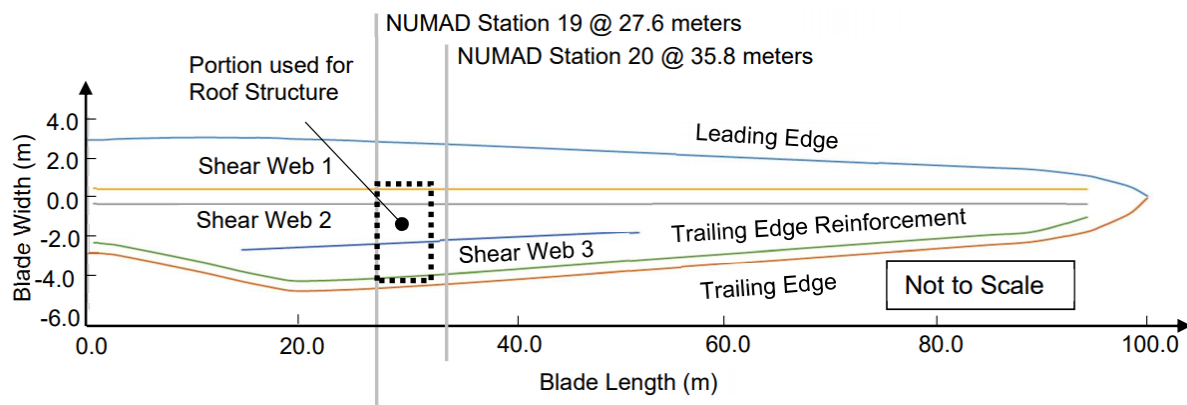
668 Figure 2



669

670

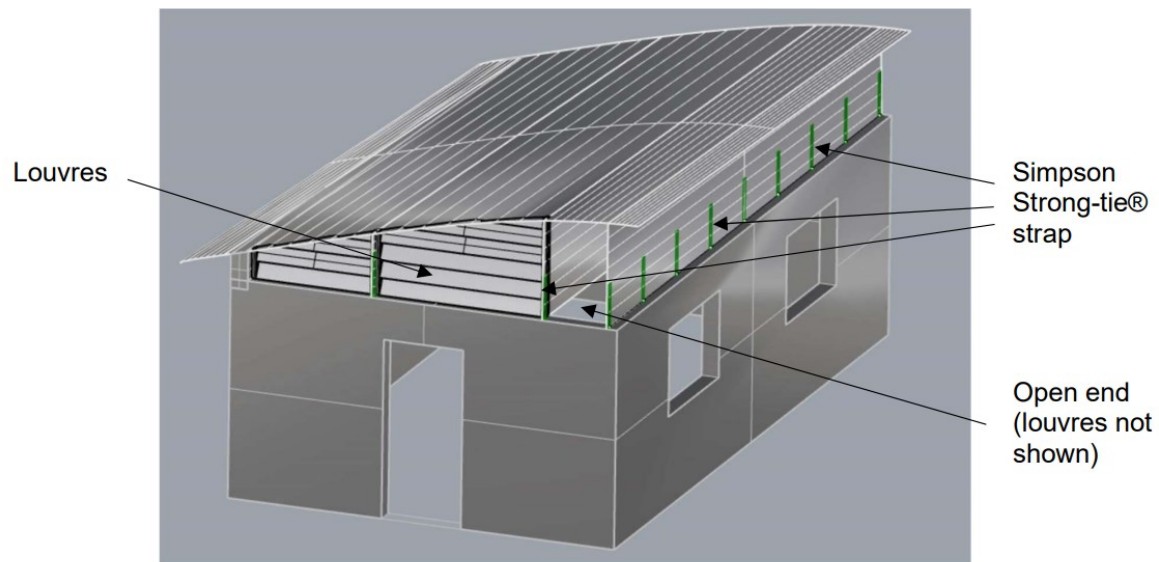
671 Figure 3



672

673

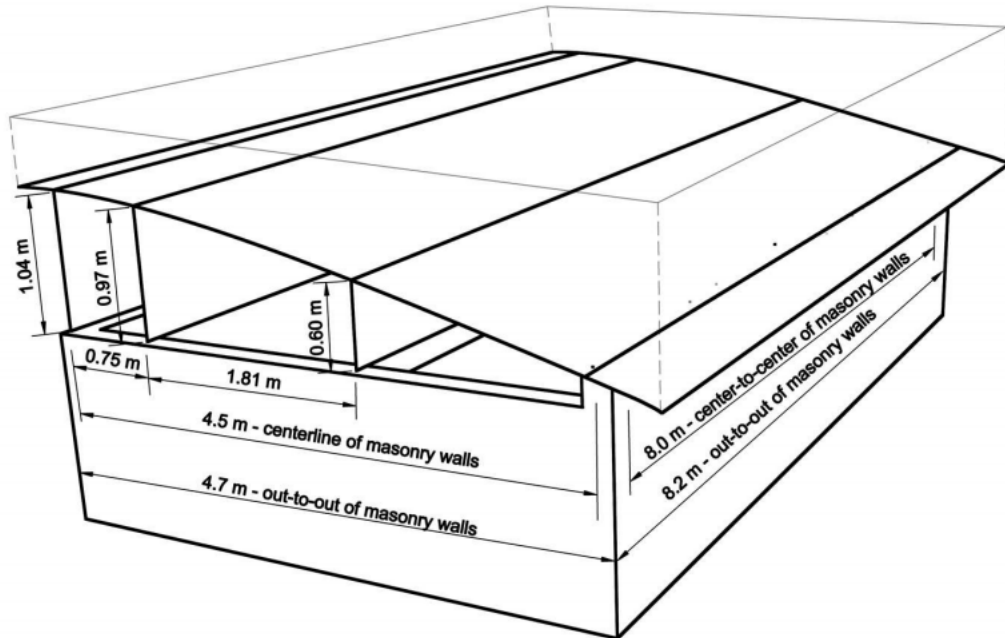
674 Figure 4



675

676

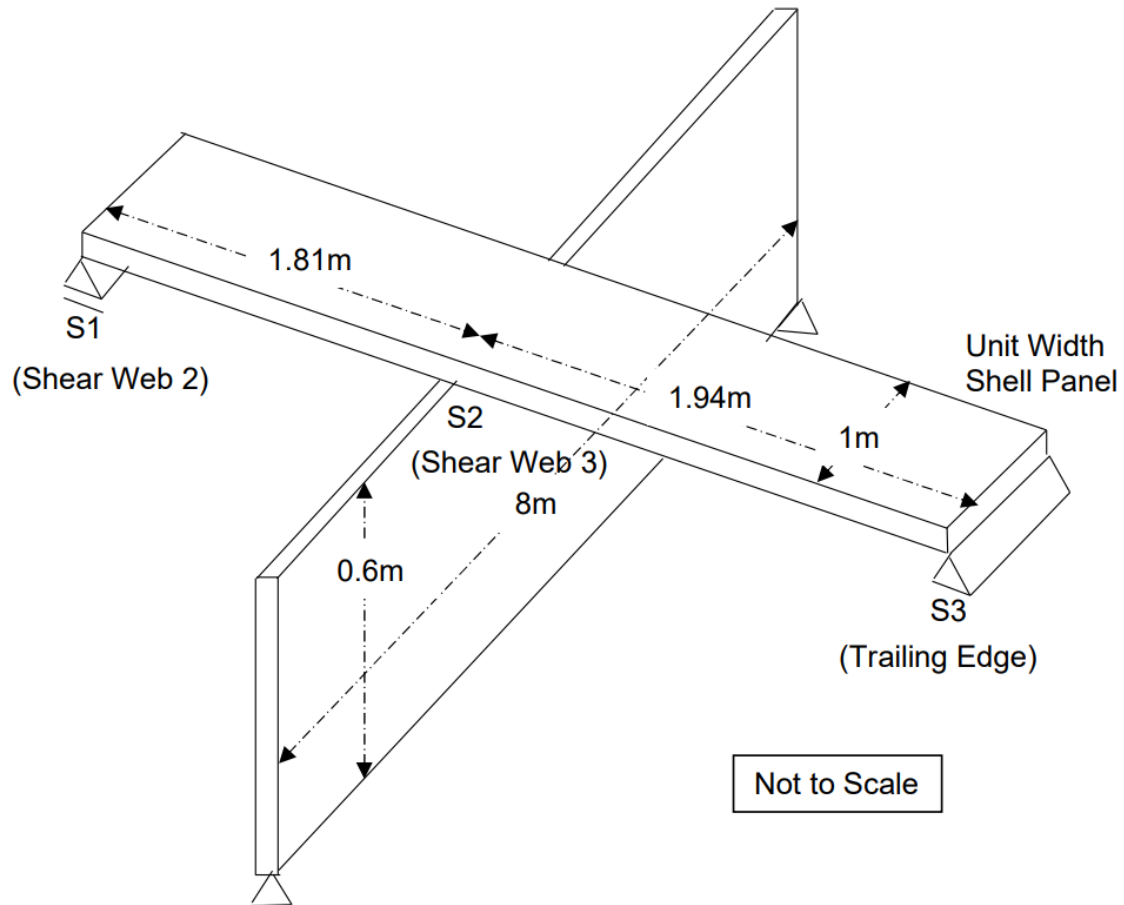
677 Figure 5



678

679

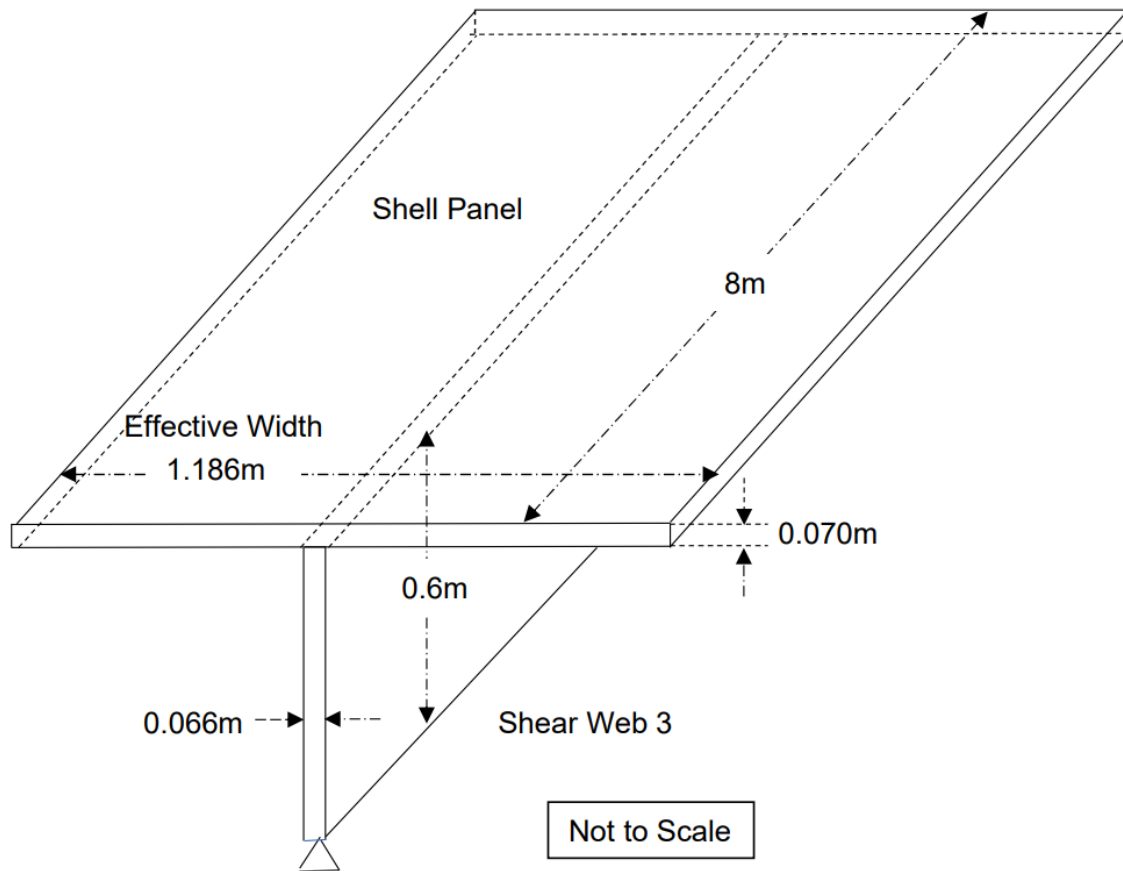
680 Figure 6



681

682

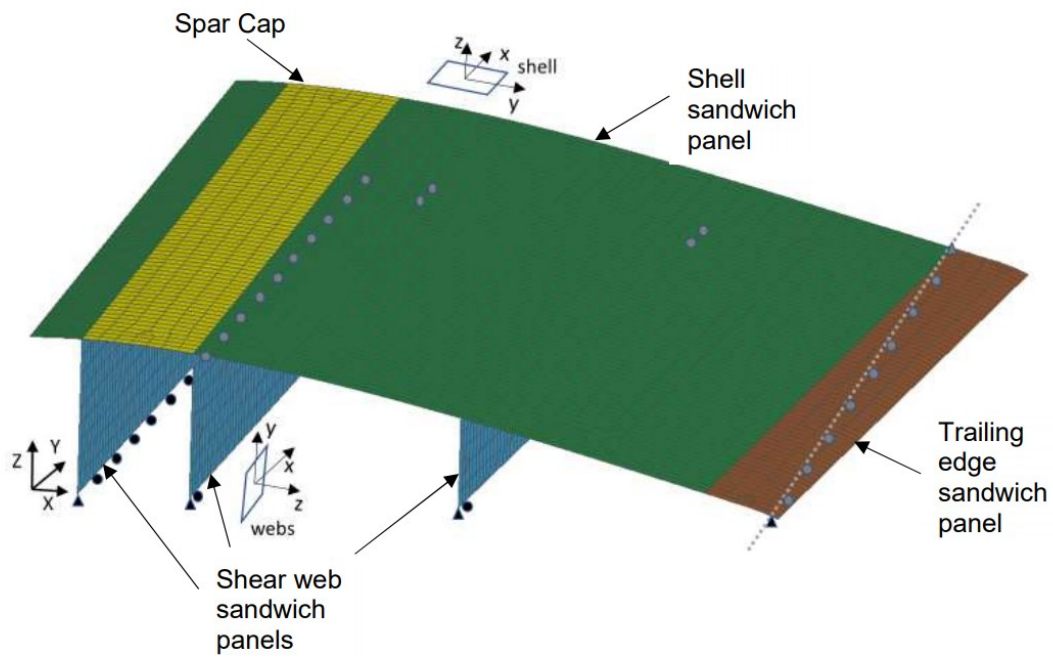
683 Figure 7



684

685

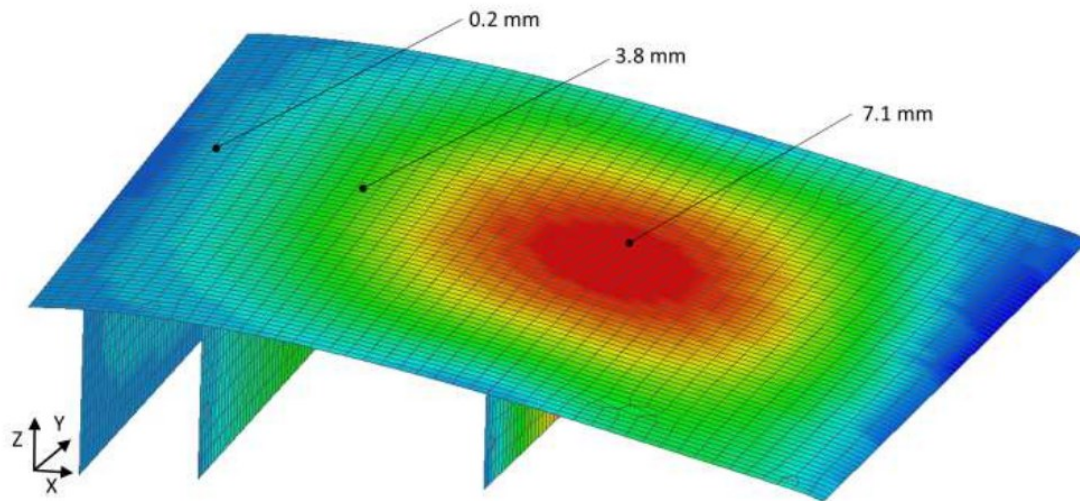
686 Figure 8



687

688

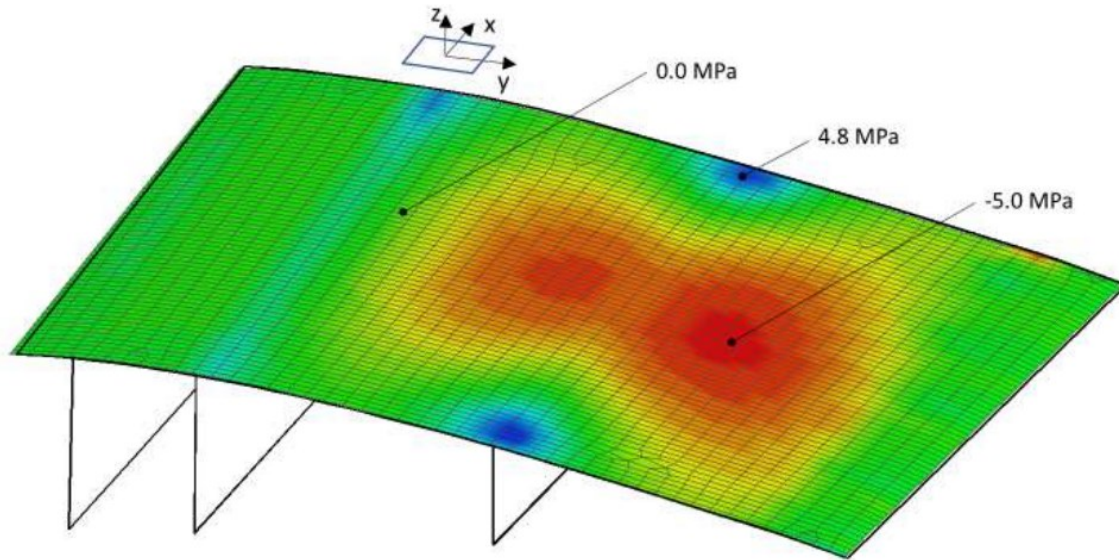
689 Figure 9



690

691

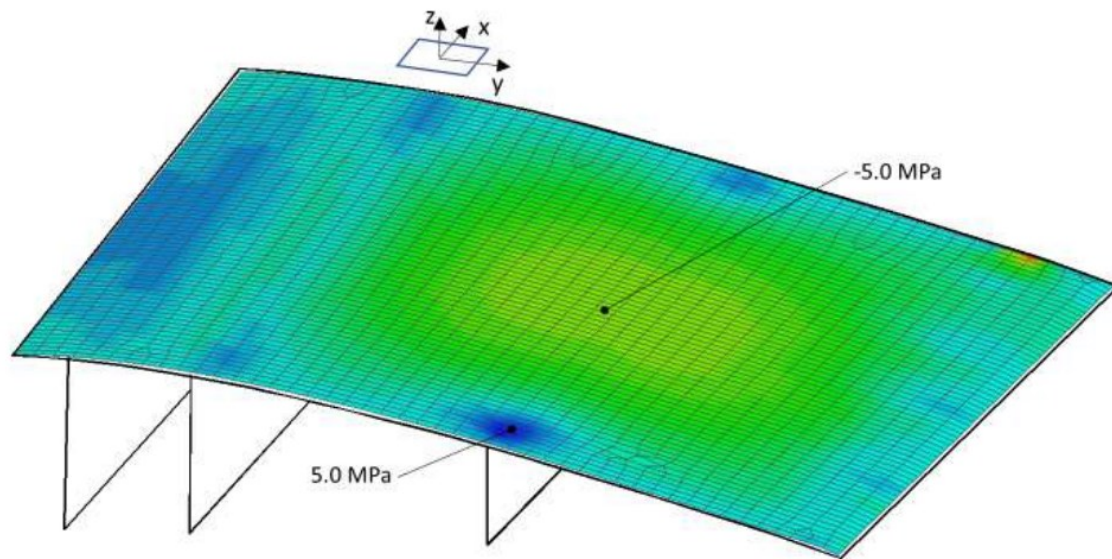
692 Figure 10



693

694

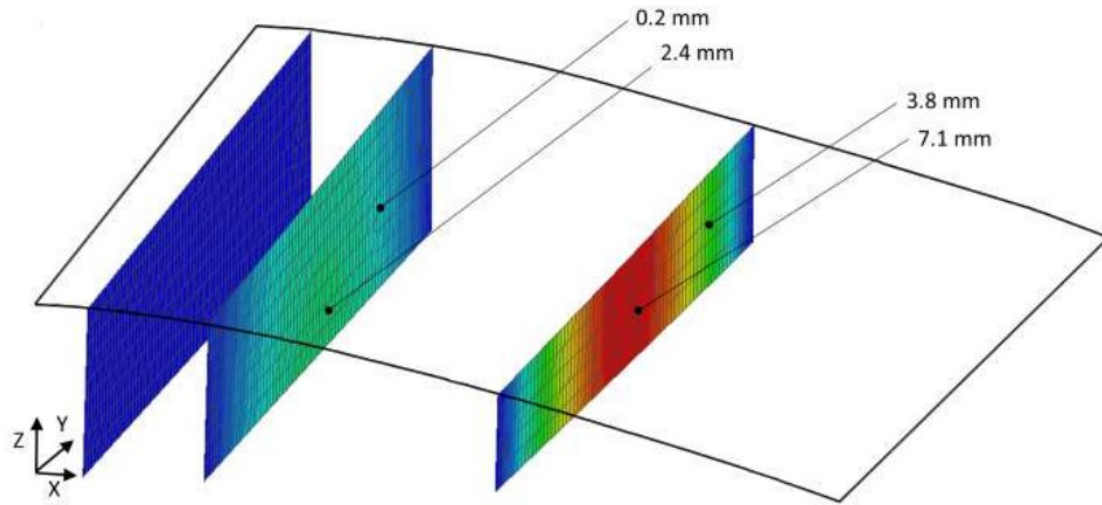
695 Figure 11



696

697

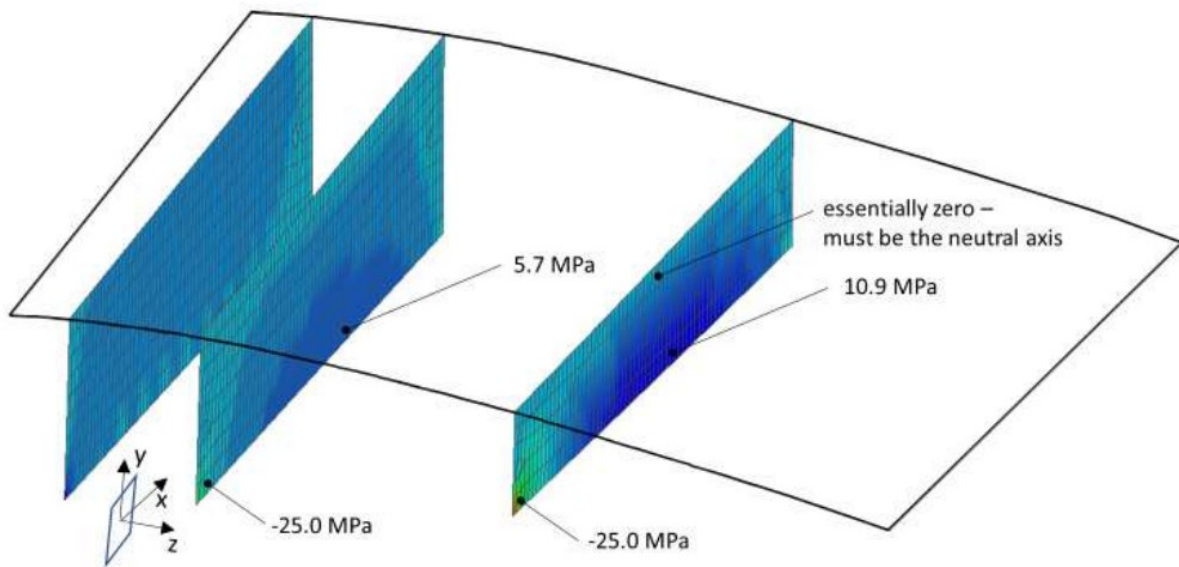
698 Figure 12



699

700

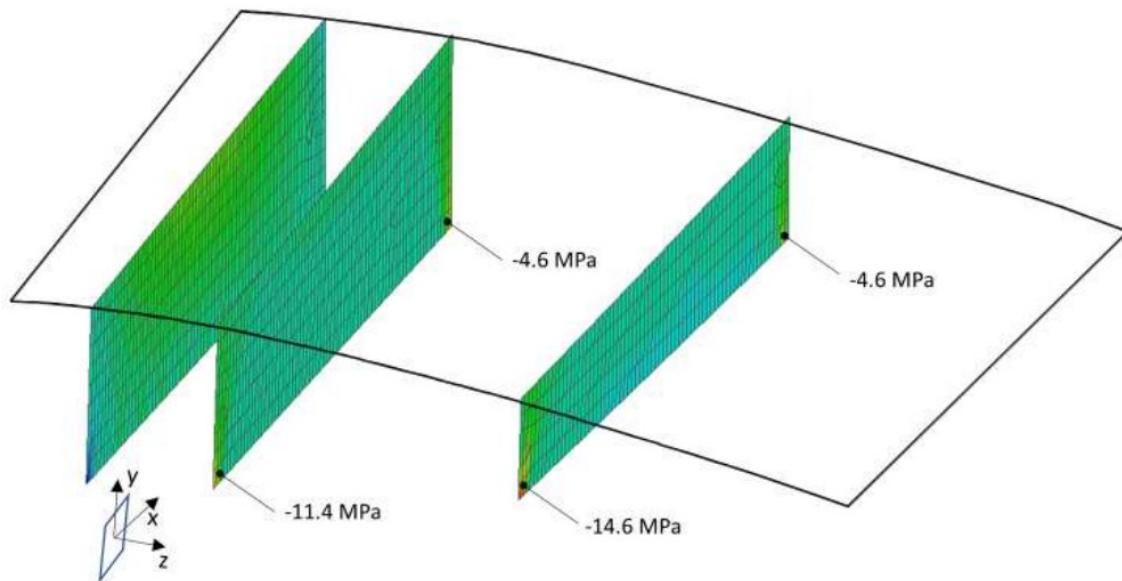
701 Figure 13



702

703

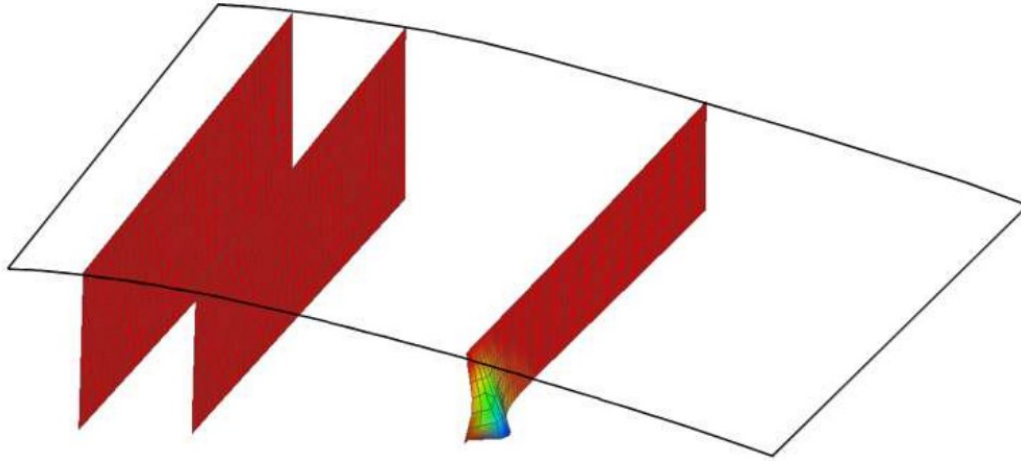
704 Figure 14



705

706

707 Figure 15



708

709

Table 1. Material properties of laminates in the SNL-100-01

| Material Type | E_{11} (GPa) | E_{22} (GPa) | G_{12} (GPa) | ν_{12} | ρ (kg/m ³) | σ_{11} (tens) (MPa) | σ_{11} (comp) (MPa) | σ_{22} (tens) (MPa) | σ_{22} (comp) (MPa) | τ (MPa) |
|--|-------------------|-------------------|-------------------|------------|--------------------------------|----------------------------------|----------------------------------|----------------------------------|----------------------------------|------------------|
| Foam | 0.256 | 0.256 | 0.022 | 0.3 | 200 | 3.1 [#] | -3.8 [#] | 3.1 [#] | -3.8 [#] | 2.0 [#] |
| Glass UD [0] ₂ | 41.80 | 14.00 | 2.63 | 0.28 | 1920 | 972 | -702 | 31 [*] | -118 [*] | 72 [*] |
| SNLBiax [±45] ₄ | 13.60 | 13.30 | 11.80 | 0.51 | 1780 | 144 | -213 | 144 | -213 | -- |
| SNLTriax [±45] ₄ [0] ₂ | 27.70 | 13.65 | 7.20 | 0.39 | 1850 | 972 | -702 | 144 [§] | -213 [§] | -- |
| SNLCarbon (UD) | 114.50 | 8.39 | 5.99 | 0.27 | 1220 | 1546 | -1047 | 52 [*] | -206 [*] | 93 [*] |
| Notes: # from AIREX [®] T92.200 (2018) * from Agarwal et al (2006) § assumes that ±45plies control strength in transverse direction -- not determined (not used in analysis) | | | | | | | | | | |

Table 2. Hand-Calculation Overdesign Factors (ODFs) for Case 1 – Shell Panel

| Stress or Displacement Component Analyzed | Hand-Calculated Value (MPa or mm) | Relevant Design Property | Ultimate Value (MPa or mm) | Partial Safety Factor (γ_M) | Code Allowable (MPa or mm) | ODF = Allowable/Calculated Values |
|---|-----------------------------------|---------------------------------|----------------------------|--------------------------------------|----------------------------|-----------------------------------|
| $\sigma_{\text{Triax_top}}$ | +5.26 | $\sigma_{22\text{tens(Triax)}}$ | +144 | 1.86 | +77.4 | 14.7 |
| $\sigma_{\text{Triax_bottom}}$ | -5.26 | $\sigma_{22\text{comp(Triax)}}$ | -213 | 1.86 | -114.5 | 21.7 |
| σ_{foam} | +0.085 | $\sigma_{\text{tens(foam)}}$ | +3.1 | 1.86 | +1.7 | 19.6 |
| σ_{foam} | -0.085 | $\sigma_{\text{comp(foam)}}$ | -3.8 | 1.86 | -2.0 | 24.0 |
| τ_{foam} | +0.045 | $\tau_{\text{ult(foam)}}$ | +2.0 | 1.86 | +1.1 | 23.9 |
| δ_{midspan} | 12.08 | L(3650)/240 | 15.6 | 1.0 | 15.6 | 1.29 |

Table 3. Hand Calculation Overdesign Factors (ODFs) for Case 2 – Shear Web (T-Beam)

| Stress or Displacement Component Analyzed | Hand-Calculated Value (MPa or mm) | Relevant Design Property | Ultimate Value (MPa or mm) | Partial Safety Factor (γ_M) | Code Allowable (MPa or mm) | ODF = Allowable/Calculated Values |
|---|-----------------------------------|---------------------------------|----------------------------|--------------------------------------|----------------------------|-----------------------------------|
| $\sigma_{\text{Triax_top}}$ | -10.06 | $\sigma_{11\text{comp(Triax)}}$ | -702 | 1.86 | -377.4 | 37.5 |
| $\sigma_{\text{Biax_skin}}$ | +36.06 | $\sigma_{11\text{tens(Biax)}}$ | +144 | 1.86 | +77.4 | 2.1 |
| $\sigma_{\text{foam_shell}}$ | -0.087 | $\sigma_{\text{comp(foam)}}$ | -3.8 | 1.86 | -2.0 | 23.0 |
| $\sigma_{\text{foam_web}}$ | -0.680 | $\sigma_{\text{comp(foam)}}$ | -3.8 | 1.86 | -2.0 | 2.9 |
| $\tau_{\text{foam_web}}$ | +0.462 | $\tau_{\text{ult(foam)}}$ | +2.0 | 1.86 | +1.1 | 2.4 |
| δ_{midspan} | 29.9 | $L(8000)/240$ | 33.3 | 1.0 | 33.3 | 1.1 |

Table 4. 3-D FEM Calculation Overdesign Factors (ODFs) for entire roof

| Stress or Displacement Component Analyzed | Hand-Calculated Value (MPa or mm) | Relevant Design Property | Ultimate Value (MPa or mm) | Partial Safety Factor (γ_M) | Code Allowable (MPa or mm) | ODF = Allowable/Calculated Values |
|---|-----------------------------------|--|----------------------------|--------------------------------------|----------------------------|-----------------------------------|
| $\sigma_{y\text{Triax_top}}$ | -5.0 | $\sigma_{11\text{comp}}(\text{Triax})$ | -702 | 1.86 | -377.4 | 75.5 |
| $\sigma_{y\text{Triax_top}}$ | +4.8 | $\sigma_{11\text{tens}}(\text{Triax})$ | +972 | 1.86 | +552.6 | 108.9 |
| $\sigma_{x\text{Triax_top}}$ | -5.0 | $\sigma_{22\text{comp}}(\text{Triax})$ | -213 | 1.86 | -114.5 | 22.9 |
| $\sigma_{x\text{Triax_top}}$ | +5.0 | $\sigma_{22\text{tens}}(\text{Triax})$ | +144 | 1.86 | +77.4 | 15.5 |
| $\sigma_{xBi\text{ax_bottom}}$ | +10.9 | $\sigma_{11\text{tens}}(\text{Bi\text{ax}})$ | +144 | 1.86 | +77.4 | 7.3 |
| $\sigma_{xBi\text{ax_bottom}}$ | -25.0 | $\sigma_{11\text{comp}}(\text{Bi\text{ax}})$ | -213 | 1.86 | -114.5 | 4.6 |
| $\sigma_{yBi\text{ax_bottom}}$ | -14.6 | $\sigma_{22\text{comp}}(\text{Bi\text{ax}})$ | -213 | 1.86 | -114.5 | 7.8 |
| δ_{shell} | 7.1 | 3750/240 | 15.6 | 1.0 | 15.6 | 2.2 |
| δ_{web} | 7.1 | 8000/240 | 33.3 | 1.0 | 33.3 | 4.7 |